Supplementary Information (SI)

A. DFT Calculation Results

The density of the electronic states resulting from each of the calculations was convoluted with Gaussian function of a typical experimental width (0.71 eV at FWHM) to simulate the PES). Figure S1 compares the results thus obtained from orbital energies[1,2] (method (i)) and from excited states of the cation[2–4] (with 2 different functionals ,method (ii)).

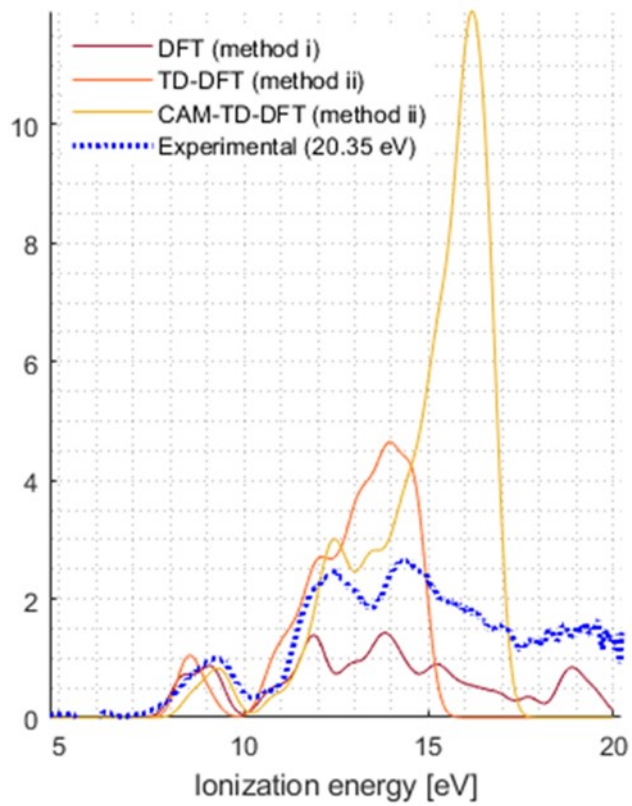

S1. Comparison of calculated spectra using different computational methods with experimental data. 40 states were used in TD-DFT while 60 were used for CAM-TD-DFT.

The calculated electronic transitions are summarized in table ST1 and assigned to the bands in the experiment.

ST1. Calculation results in comparison to the experimental values for mainly the first 3 bands

Band	Ionization Energies [eV]			
	DFT	TD-DFT	TD-CAM-DFT	Experimental (±0.3 eV)
0	8.22	8.4013	8.5955	9.2
	8.4	8.4845	9.07	
	8.87	8.5628	9.3202	

	9.12	9.0086	9.5495	
	9.29			
1	10.64	10.644	10.821	12.2
	11.09	10.854	11.464	
	11.53	11.002	11.557	
	11.75	11.264	11.93	
	11.91	11.381	12.057	
	12.01	11.445	12.095	
	12.07	11.783	12.186	
		11.807	12.294	
		11.874	12.367	
		11.954	12.438	
		11.987	12.495	
		12.038	12.54	
		12.196	12.598	
		12.36	12.72	
		12.429	12.82	
		12.458	12.922	
		12.521	13.056	
		12.742	13.246	
		12.797	13.345	
		12.886	13.358	
		12.974	13.42	
		12.994	13.508	
		13.044	13.559	
		13.105	13.614	
		13.175		
		13.239		
		13.265		
		13.323		
2	12.68	13.481	13.828	14.4
	12.87	13.495	13.932	
	13.13	13.554	13.99	
	13.47	13.609	14.087	
	13.67	13.694	14.119	
	13.75	13.741	14.247	
	13.92	13.812	14.257	
	14.1	13.828	14.293	
	14.31	13.916	14.419	
	14.63	13.962	14.468	
		13.975	14.559	
		14.05	14.592	

		14.072	14.625	
		14.081	14.627	
		14.103	14.731	
		14.195	14.799	
		14.311	14.844	
		14.459	14.906	
		14.483	15.054	
		14.52	15.056	
		14.576	15.06	
		14.585	15.125	
		14.615	15.148	
		14.695	15.166	
		14.754	15.179	
		14.765	15.202	
		14.785	15.222	
		14.806	15.278	
			15.321	
			15.356	
			15.386	
			15.445	
			15.506	
			15.517	
			15.53	
			15.539	
			15.602	
			15.622	
	15.11		15.699	Higher IE bands
	15.2		15.735	
	15.53		15.752	
	15.94		15.797	
	16.4		15.817	
	16.94		15.833	
	17.72		15.863	
	18.63		15.877	
	18.84		15.902	
	19.09		15.917	
	19.55		15.948	
	21.47		15.999	
	22.4		16.005	
	22.54		16.025	
	22.73		16.037	
	23.32		16.05	

	25.39		16.055	
	25.6		16.072	
	30.56		16.096	
	31.3		16.11	
	31.55		16.116	
			16.125	
			16.134	
			16.141	
			16.165	
			16.184	
			16.205	
			16.221	
			16.27	
			16.289	
			16.292	
			16.311	
			16.336	
			16.352	
			16.361	
			16.439	
			16.448	
			16.476	
			16.491	
			16.504	
			16.537	
			16.549	
			16.557	
			16.569	
			16.626	
			16.634	
			16.658	
			16.68	
			16.692	
			16.718	
			16.722	
			16.734	
			16.763	
			16.774	

B. Experimental Resolution

The table-top HHG spectrometer allows a scan of the generated harmonics by rotation of the grating as described in previous work[5–8] and by Polleto and co-workers[9,10]. An example spectrum of such a scan with Gaussian functions fitted to the different harmonics used in this study is presented in Figure S2 (fit results can be found in Table ST2). Note that the PES were not necessarily measured at the peak positions of each harmonic, mainly to minimize the leaking from an adjacent harmonic.

ST2. Results for Gaussian functions fits to HH scan by grating rotation.

HH#	hv at peak [eV]	80% of FWHM [eV]
11	17.05	0.60
13	20.19	0.78
15	23.29	1.01
17	26.40	1.21
19	29.53	1.68
21	32.55	1.65
23	35.92	3.02
25	40.00	3.45

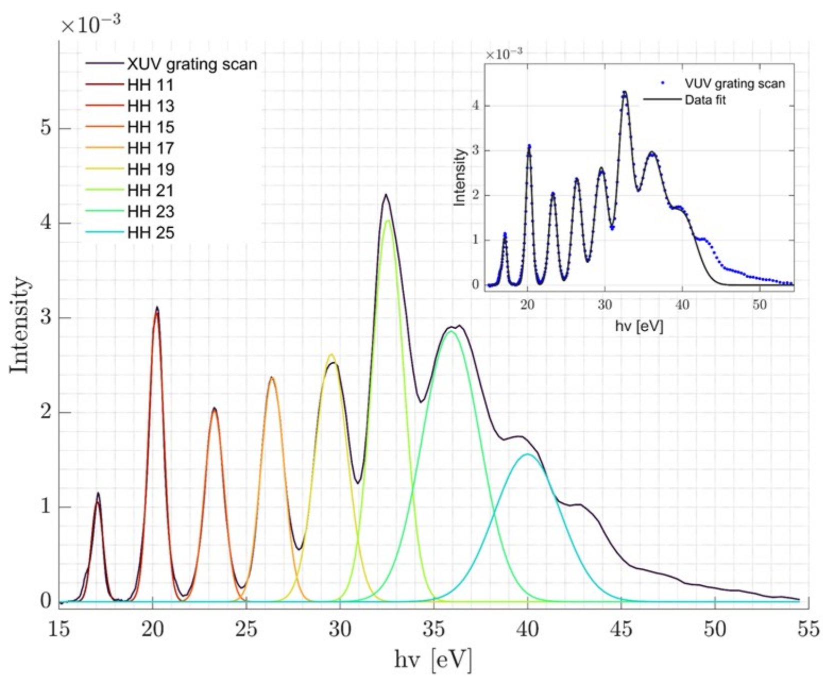

S2. Scan of the grating of the monochromator in the high harmonic setup.

The fit to the trace measured by scanning the grating in the HHG experimental setup reveals the variance in widths of the generated harmonics and shows the expected broadening with the increasing order of the harmonic[11,12].

The widths measured from the fits to He peak in the EUV PES measurements (at VBE=24.7 eV) however, provide information about the experimental resolution for a given photon energy. These results are shown in table ST3. The experimental uncertainty for the EUV photon energy is estimated by the average half width of the Gaussians (at 80% of FWHM) and equals to 0.3 eV.

ST3. Results for Gaussian functions fits to helium peak in spectra of different photon energies

HH#	hv [eV]	He Peak at 80% of FWHM [eV]	Number of measurements taken for average
17	26.5	0.56	4
19	29.7	0.57	3
21	32.7	0.60	5
23	35.7	0.61	4

C. Fitted PES and Onset Energies

The fit to the EUV-PES is shown in S3. The fitted traces are a sum of multi-component Gaussian fit. Table ST4 gives a summary of the Gaussians fits for Bands 0-2. The increase in widths of Band 0 and 1 is due to the monochromator resolution.

ST4. Results for Gaussian Fits for Bands 0-2

Photon energy [eV]	Band 0		Band 1		Band 2	
	VBE [eV]	0.8·FWHM [eV]	VBE [eV]	0.8·FWHM [eV]	VBE [eV]	0.8·FWHM [eV]
17.2	9.21	1.34	12.21	1.41	14.34	1.70
20.4	9.10	1.35	12.28	1.54	14.49	1.58
23.5	9.15	1.46	12.22	1.47	14.50	1.80
26.5	9.01	1.62	12.01	1.54	14.25	1.75
29.7	9.16	1.64	12.29	1.65	14.58	1.80
32.7	9.35	1.80	12.34	1.80	14.56	1.80
35.7	9.13	1.80	12.16	1.80	14.31	1.78
Average ± STD	**9.2±0.1**		**12.2±0.1**		**14.4±0.1**	

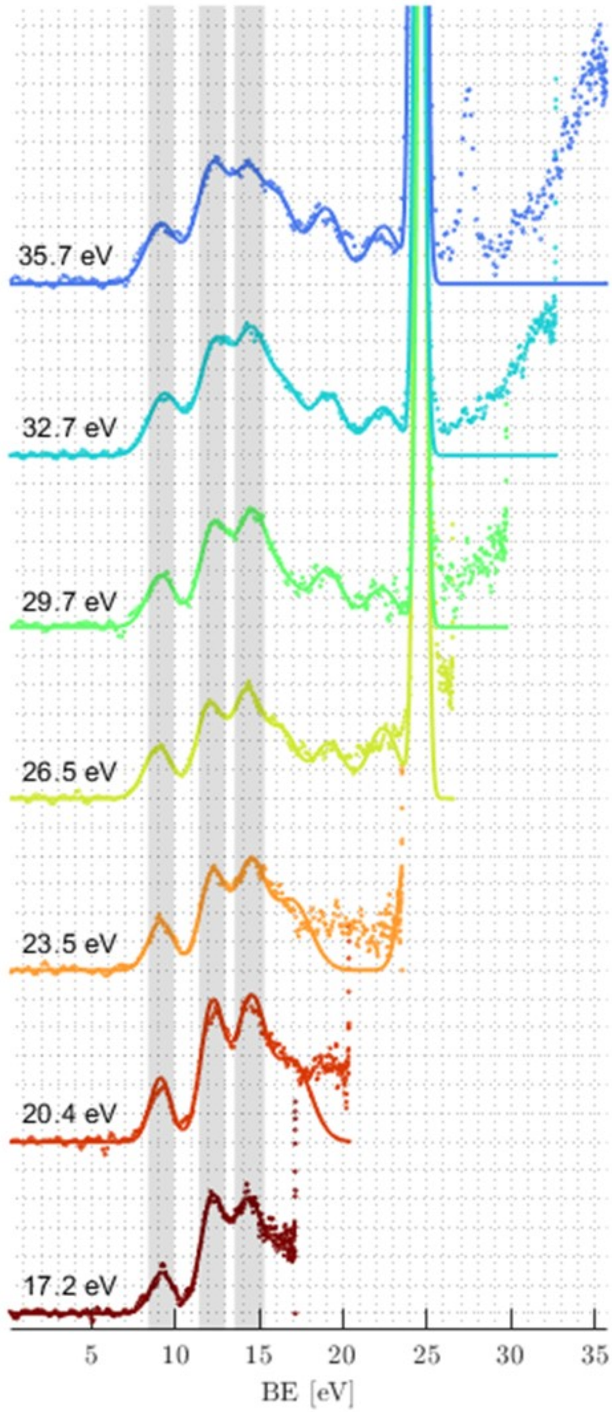

S3. EUV PES with indication of the photon energies and the fitted spectra (full lines). The grey shades indicate Bands 0-2.

The intersection between linear fits to the rising edge of the signal and the baseline, see Figure S4, were used to determine AE for each PES trace. The results are summarized in Table ST5 and shown in Figure S4. Based on the Gaussian fit results for Band 0 in Table ST4, we see the monochromator has the best resolution for the 3 lowest harmonics. Hence, we deduce the appearance energy for the EUV case from the data taken with the latter as presented in the Table ST5 and Figure S4 below.

ST5. Appearance energy determination from EUV data

hv [eV]	**onset [eV]**
17.2	7.76
20.4	7.84
23.5	7.63
Average ± STD	7.7±0.1

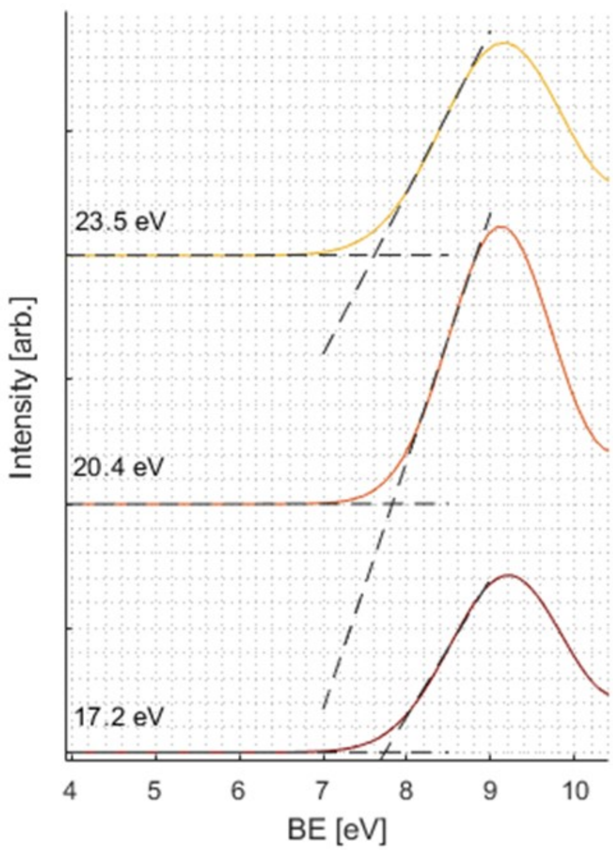

S4. Linear fits to baseline and steepest signal increase for EUV PES data analyzed for the estimation of the appearance energy from EUV.

D. List of Abbreviations

AE	appearance energies
AIE	adiabatic ionization energy
BE	binding energy
BP	benzophenone
CCD	charge-coupled device
EL	Even-Lavie
EUV	extreme ultraviolet
FWHM	full width half maximum
GC-MS	gas-chromatography mass-spectrometry
He	helium
HHG	high harmonic generation
IE	ionization energies
KE	kinetic energy
MB	molecular beam
MCP	microchannel plate
MPI	multi-photon ionization
MS	mass spectra
OB	Oxybenzone
PAD	photoelectron angular distributions
PES	photoelectron spectra
PS	phosphor screen
SI	supplementary information
SNR	signal to noise ratio
STD	standard deviation
(TD-)DFT	(time dependent-) density function theory
UV	266 nm light
VBE	vertical binding energies
VIE	vertical ionization energies
VIS	400 nm light
VMI	velocity-map imaging

Bibliography

1 D. P. Chong, O. V. Gritsenko and E. J. Baerends, Interpretation of the Kohn-Sham orbital energies as approximate vertical ionization potentials, *J. Chem. Phys.*, 2002, **116**, 1760–1772.

2 V. Lemierre, A. Chrostowska, A. Dargelos and H. Chermette, Calculation of ionization potentials of small molecules: A comparative study of different methods, *J. Phys. Chem. A*, 2005, **109**, 8348–8355.

3 D. A. Horke and J. R. R. Verlet, Photoelectron spectroscopy of the model GFP chromophore anion, *Phys. Chem. Chem. Phys.*, 2012, **14**, 8511–8515.

4 O. Tau, A. Henley, A. N. Boichenko, N. N. Kleshchina, R. Riley, B. Wang, D. Winning, R. Lewin, I. P. Parkin, J. M. Ward, H. C. Hailes, A. V. Bochenkova and H. H. Fielding, Liquid-microjet photoelectron spectroscopy of the green fluorescent protein chromophore, *Nat. Commun.*, 2022, **13**, 1–7.

5 T. E. Gartmann, S. Hartweg, L. Ban, E. Chasovskikh, B. L. Yoder and R. Signorell, Electron scattering in large water clusters from photoelectron imaging with high harmonic radiation, *Phys. Chem. Chem. Phys.*, 2018, **20**, 16364–16371.

6 L. Ban, C. W. West, E. Chasovskikh, T. E. Gartmann, B. L. Yoder and R. Signorell, Below Band Gap Formation of Solvated Electrons in Neutral Water Clusters?, *J. Phys. Chem. A*, 2020, **124**, 7959–7965.

7 T. E. Gartmann, L. Ban, B. L. Yoder, S. Hartweg, E. Chasovskikh and R. Signorell, Relaxation dynamics and genuine properties of the solvated electron in neutral water Clusters, *J. Phys. Chem. Lett.*, 2019, **10**, 4777–4782.

8 L. Ban, B. L. Yoder and R. Signorell, Size-Resolved Electron Solvation in Neutral Water Clusters, *J. Phys. Chem. A*, 2021, **125**, 5326–5334.

9 F. Frassetto, C. Cacho, C. A. Froud, I. C. E. Turcu, P. Villoresi, W. A. Bryan, E. Springate and L. Poletto, Single-grating monochromator for extreme-ultraviolet ultrashort pulses, *Opt. Express*, 2011, **19**, 19169.

10 F. Frassetto, P. Miotti and L. Poletto, Grating Configurations for the Spectral Selection of Coherent Ultrashort Pulses in the Extreme-Ultraviolet, *Photonics*, 2014, **1**, 442–454.

11 P. Salières and M. Lewenstein, Generation of ultrashort coherent XUV pulses by harmonic conversion of intense laser pulses in gases: Towards attosecond pulses, *Meas. Sci. Technol.*, 2001, **12**, 1818–1827.

12 I. J. Sola, A. Zaïr, R. López-Martens, P. Johnsson, K. Varjú, E. Cormier, J. Mauritsson, A. L'Huillier, V. Strelkov, E. Mével and E. Constant, Temporal and spectral studies of high-order harmonics generated by polarization-modulated infrared fields, *Phys. Rev. A - At. Mol. Opt. Phys.*, 2006, **74**, 013810.